Carboxyl-Terminus Determinants of the Iron Transporter DMT1/SLC11A2 Isoform II (−IRE/1B) Mediate Internalization from the Plasma Membrane into Recycling Endosomes

Steven Lam-Yuk-Tseung,[‡] Nicolas Touret,[§] Sergio Grinstein,[§] and Philippe Gros*,[‡]

Department of Biochemistry, McGill Cancer Center and Center for Host Resistance, McGill University, Montreal, Quebec H3G 1Y6, Canada, and Program in Cell Biology, Hospital for Sick Children, Toronto, Ontario M5G 1X8, Canada

Received May 17, 2005; Revised Manuscript Received July 10, 2005

ABSTRACT: Mutations in *DMT1* (*Nramp2* and *Slc11a2*) impair iron metabolism and cause microcytic anemia. DMT1 is expressed at the duodenal brush border where it controls uptake of dietary iron and is present at the plasma membrane and in recycling endosomes of most cells, where it is necessary for acquisition of transferrin-associated iron. The goal of this study was to identify signal(s) in the cytoplasmic segments of DMT1 responsible for its subcellular targeting and internalization from the plasma membrane into recycling endosomes. We introduced mutations in the amino terminus (ΔNT), carboxyl terminus (ΔCT), as well as in $NPAY^{28-31}$, $YSCF^{62-65}$, and $YLLNT^{555-559}$ motifs of a DMT1 construct bearing an exofacial epitope tag, which allowed labeling of the transporter at the cell surface for kinetic studies. Mutants were stably expressed in LLC-PK_1 kidney cells and were studied for transport activity, subcellular localization, cell-surface and recycling pool distribution, and internalization from the plasma membrane. Kinetic studies showed that carboxyl-terminus mutants (ΔCT and ΔYLLNT) had an increased fraction of the "recycling pool" that was expressed at the cell surface because of impaired internalization from the plasma membrane. Further cell-surface-labeling and immunofluorescence studies in intact cells showed that the ΔYLLNT and ΔCT mutants were targeted to the lysosomal compartment upon internalization. These results suggest that the major signal for internalization and recycling of DMT1 isoform II (−IRE/1B) resides in its carboxyl terminus and that removal of this signal leads to a default lysosomal targeting.

The divalent metal transporter 1 (DMT1,[1] also known as Nramp2, DCT1, and Slc11a2) plays a dual role in intestinal iron acquisition and in iron uptake by peripheral tissues. DMT1 is part of a large family of highly conserved metal transporters. It is an integral membrane phosphoglycoprotein consisting of 12 putative transmembrane (TM) domains, with the predicted amino and carboxyl termini positioned on the intracytoplasmic side of the membrane. Studies in *Xenopus* oocytes and transfected mammalian cell lines have demonstrated that DMT1 transports a number of divalent metals (Fe^{2+}, Mn^{2+}, Co^{2+}, Cu^{2+}, Cd^{2+}, Ni^{2+}, Pb^{2+}, and Zn^{2+}) in a pH-dependent fashion by a proton cotransport mechanism (*1*−*3*). DMT1 is expressed at the brush border of the absorptive epithelium of duodenal villi (*4*), where it is responsible for the uptake of non-heme dietary iron following reduction from its ferric (Fe^{3+}) to ferrous (Fe^{2+}) state by a ferric reductase. In nonepithelial cells, iron absorption occurs through internalization of transferrin-bound iron via the transferrin-receptor pathway. DMT1 is also expressed at the plasma membrane and in transferrin-positive recycling endosomes of most cells and tissues (*1*, *5*). It catalyzes the efflux of iron from acidified endosomes, across the endosomal membrane into the cytosol (*6*). Vacuolar ATPase-mediated endosomal acidification simultaneously facilitates the release of iron from transferrin and provides the pH gradient required for DMT1 function (*7*). Naturally occurring mutations in *DMT1* cause severe iron deficiency and microcytic anemia in *mk* mice and *Belgrade* rats (*8*, *9*). Both mutants show the same alteration (G185R) in predicted TM4 of DMT1, which abrogates both intestinal iron absorption and endosomal transport of transferrin−iron (*10*−*14*). Finally, DMT1 is also expressed at the brush border of epithelial cells of proximal tubules of the kidney (*15*), where it may function as a re-uptake system for divalent metals.

The *DMT1* gene produces at least two distinct mRNAs by alternative splicing of two 3′ exons encoding different 3′ untranslated regions (UTR) and protein products with distinct C termini (*16*, *17*). *DMT1* isoform I (+IRE) contains an iron-responsive element (IRE) in its 3′ UTR. DMT1 isoform I is expressed at the brush border of duodenal enterocytes where its expression is induced by dietary iron depravation (*4*, *18*). DMT1 isoform I is also expressed in the kidney (*4*, *15*). DMT1 isoform II (−IRE) lacks an IRE and encodes a protein that has a different C-terminal 25 amino acid segment. DMT1 isoform II is expressed preferentially in nonepithelial cells and is very abundant in reticulocytes (*19*). Recently, ad-

* To whom correspondence should be addressed: Department of Biochemistry, McGill University, 3655 Promenade Sir William Osler, Montreal, Quebec H3G 1Y6, Canada. E-mail: philippe.gros@mcgill.ca. Telephone: (514) 398-7291. Fax: (514) 398-2603.

[‡] McGill University.

[§] Hospital for Sick Children.

[1] Abbreviations: DMT1, divalent metal transporter 1; Nramp2, natural resistance-associated macrophage protein 2; TM, transmembrane; IRE, iron responsive element; Lamp, lysosomal-associated membrane protein; CFTR, cystic fibrosis transmembrane conductance regulator; HA, hemaglutinin; OPD, *o*-phenylenediamine dihydrochloride; HRP, horseradish peroxidase; GFP, green fluorescent protein; MESNA, 2-mercaptoethane sulfonate; EEA1, early endosome antigen 1; MNK, Menkes; GLUT4, glucose transporter 4.

10.1021/bi050911r CCC: $30.25
Published on Web 08/17/2005

ditional isoforms of DMT1 mRNAs have been identified based on alternate promoter usage at *DMT1* exon 1 (exon 1A versus 1B) (*17*). This alternate promoter usage is predicted to produce a DMT1 protein bearing an additional 29 amino acids (exon 1A) upstream of the previously identified start codon of DMT1 isoforms I and II (exon 1B). The role of these additional residues in the expression, function, and targeting of DMT1 has not yet been studied. Touret and colleagues have demonstrated that DMT1 isoform II, when expressed in transfected CHO and LLC-PK_1 cells, is present at the plasma membrane and in an acidic transferrin receptor-positive endomembrane vesicular compartment. Kinetic studies of an exofacially tagged DMT1 molecule showed similar amounts of protein in endomembrane compartment-(s) and at the cell surface. The two components are in dynamic equilibrium, with surface transporters being continuously internalized via a clathrin and dynamin-dependent process (*7*). Therefore, proper physiological function of DMT1 in iron metabolism involves not only proper targeting to the plasma membrane but also requires efficient internalization and recycling via recycling endosomes.

Tyrosine-based motifs (NPXY and YXXϕ, where ϕ = bulky hydrophobic) have been shown to act as internalization signals for clathrin-mediated endocytosis (*20*). The NPXY motif was initially discovered as a mutation (Y807C) in the cytoplasmic domain of the LDL receptor that abolishes internalization of the receptor (*21*) in a patient with familial hypercholsterolemia. Mutagenesis studies (*22*) showed that NPXY is an internalization signal for surface proteins such as the LDL receptor-related protein 1 (LRP1) (*23*), the EGF receptor (*24*), and megalin (*25*). Several proteins, including clathrin, AP-2, and Dab2, appear to function as recognition proteins for NPXY signals (*20*). The YXXϕ motif has also been shown to act as a plasma-membrane internalization motif for endocytic receptors such as the transferrin receptor and ion transporters such as the cystic fibrosis transmembrane conductance regulator (CFTR) (*20*). YXXϕ motifs have also been implicated in targeting membrane proteins such as LAMP-1 and LAMP-2 to lysosomes. YXXϕ signals interact with the μ subunits of AP-1 and AP-2 complexes, which in turn recruit clathrin molecules (*26*−*28*). Cytoplasmic dileucine-based (LL) motifs of membrane proteins (such as GLUT4) have also been shown to act as signals leading to clathrin-mediated endocytosis or targeting to endosomal−lysosomal compartments (*20*). Residues neighboring the LL signals appear to dictate whether clathrin recruitment occurs via AP complexes or via ARF-dependent clathrin adaptors.

Examination of the sequence of proposed cytoplasmic domains of DMT1 reveals the presence of three putative internalization motifs: two tyrosine-based motifs of the forms NPXY and YXXϕ ($NPAY^{28-31}$ and $YSCF^{62-65}$) in the amino-terminal region and a dileucine motif ($LL^{556,557}$) in the carboxyl-terminal region. In the present study, we sought to identify the specific signal(s) in the cytoplasmic segments of DMT1 isoform II responsible for internalization and recycling of the transporter from the plasma membrane.

MATERIALS AND METHODS

Materials. Reagent-grade chemicals were purchased from Sigma Chemical (St. Louis, MO). Monoclonal mouse antibody (Ab) HA.11 directed against the influenza hemagglutinin epitope (HA) was purchased from Covance (Princeton, NJ). Cy2- and Cy3-labeled anti-mouse antibodies and HRP-coupled donkey anti-mouse antisera were purchased from Jackson ImmunoResearch Laboratories (West Grove, PA). The plasmid-encoding GFP-fusion protein GFP-syntaxin 13 was the kind gift from Dr. D. Williams (Department of Biochemistry, University of Toronto, Toronto, Canada). The GFP-Lamp1 plasmid was a kind gift from Dr. Patrice Boquet (Institut National de la Santé et de la Recherché Médicale, France).

Table 1: Oligonucleotides Used for Mutagenesis[a]

primer name	nucleotide sequence (5′−3′)
ΔNPAY For	ccttggcgccatcagcaactcatccc
ΔYSCF For	cctgaggaggagagctttcgtaaac
ΔYLLNT For	gctcagcctgaactcgtggatgctgactcag
ΔNT For	ccgctcgaggccacc**atg**ctgaaactctgggcgttcacggggc
ΔCT Rev	cggaattctt<u>aa</u>cccaatgcaatcaaacactgc

[a] For indicates forward, and Rev indicates reverse. Bold type indicates the inserted initiator methionine codon for ΔNT. The inserted stop codon for ΔCT is underlined.

Table 2: Summary of Subcellular Localization of WT and Mutant DMT1-HA

	plasma membrane	recycling endosomes	late endosome/ lysosome	endoplasmic reticulum
WT	+	+	−	−
ΔNPAY	+	+	−	−
ΔYSCF	+	+	−	−
ΔYLLNT	+	−	+	−
ΔNT	−	−	−	+
ΔCT	+	−	+	−

Plasmids and Constructs. Full-length murine *DMT1* (*Nramp2*, *DCT1*, and *Slc11a2*; GenBank accession number L33415) isoform II (non-IRE, isoform 1B) cDNA was modified by the in-frame addition of an HA epitope at amino acid position 330, as previously described (*2*). Deletion and truncation mutations in DMT1-HA were created by site-directed mutagenesis using oligonucleotide primers listed in Table 1 by a recombinant polymerase chain reaction protocol (*29*). For ΔNT, a primer was designed to delete the first 67 amino acids of DMT1, up to the first membrane-spanning segment, with the addition of an initiator methionine (Table 1). For ΔCT, a primer was designed to remove 34 amino acids from the carboxyl terminus of DMT1, with the insertion of a stop codon after G534 and an *EcoR* I site for subsequent cloning. Mutants were constructed into the mammalian expression vector, pCB6, using restriction enzyme sites *Xho* I and *BstE* II for mutants ΔNPAY, ΔYSCF, and ΔNT and sites *Sac* I and *EcoR* I for mutants ΔYLLNT and ΔCT.

Cell Culture, Transfection, and Immunoblotting. LLC-PK_1 cells were grown at 37 °C in a 5% CO_2 incubator in Dulbecco's modified Eagle's medium (Invitrogen) supplemented with 10% fetal bovine serum (growth media). LLC-PK_1 cells were transfected with DMT1-HA/pCB6 vectors using a calcium−phosphate coprecipitation method. Selection of stably transfected clones was done using 1.4 mg/mL G418 (Invitrogen) for 10−14 days. Individual colonies were then picked and expanded. Total cell lysates were prepared and separated by SDS−PAGE. Clones showing robust DMT1-HA expression were identified by immunoblotting with mouse anti-HA antibody, as previously described (*30*).

Calcein Divalent Metal-Transport Assay. Calcein acetoxymethylester (calcein-AM, Molecular Probes) was pre-

pared as a 500 μM stock solution in dimethyl sulfoxide. Fe^{2+} and Co^{2+} solutions were freshly prepared in deionized water as 2 mM stock solutions of ferrous ammonium sulfate and cobalt chloride, respectively. Measurement of Fe^{2+} and Co^{2+} transport in DMT1-HA-transfected LLC-PK_1 cells was done using a fluorescence quenching assay, exactly as we have previously described with CHO cells (*2*). Initial rates of metal transport were calculated from the fluorescence quenching curves, and results for each transfectant were normalized to activity of wild-type DMT1-HA-expressing cells.

ELISA. For all ELISA assays, 2.8×10^5 cells/well were seeded in 48-well tissue culture plates and grown to confluency (16−24 h). Cells were fixed in phosphate-buffered saline (PBS) containing 4% paraformaldehyde for 30 min at 20 °C. Blocking, permeablization, and incubations with the antibody were carried out at 37 °C. A solution of 5% nonfat milk in PBS was used for blocking and dilution of all antibodies unless otherwise noted. Washes were performed 3 times with PBS containing 1 mM $MgCl_2$ and 0.1 mM $CaCl_2$ (PBS++). After donkey anti-mouse-HRP secondary Ab incubation, peroxidase activity was detected by incubating cells with HRP substrate [0.4 mg/mL *o*-phenylenediamine dihydrochloride (OPD), Sigma *FAST* OPD; 550 μL/well] according to the instructions of the manufacturer. Reactions were stopped with 150 μL of 3 M HCl/well, and absorbance readings (492 nm) were taken with a spectrometer. For all assays, background absorbance readings from (a) nonspecific binding of secondary Ab and (b) nonspecific binding of primary Ab to vector-transfected cells were subtracted for each sample.

For quantification of cell-surface expression of DMT1-HA at steady state, cells were washed with cold PBS++, fixed, blocked, incubated with anti-HA Ab (1:500) for 90 min, washed, and permeabilized 30 min in 0.1% Triton X-100/PBS. Cells were blocked for 30 min and labeled with secondary Ab (donkey anti-mouse-HRP Ab, 1:4000) for 1 h. For quantification of total DMT1-HA expression, cells were permeabilized prior to incubation with anti-HA Ab. Cell-surface readings were normalized to total DMT1-HA values for each cell clone and were expressed as a percentage.

To quantify cell-surface DMT1-HA expression as a percentage of the recycling pool, cells were incubated in anti-HA Ab (1:200) diluted in 2% nonfat milk/RPMI for 3 h at 37 °C. To measure surface DMT1-HA molecules, cells were washed with PBS, fixed, blocked, and incubated with secondary Ab. To measure recycling pool DMT1-HA, cells were sequentially permeabilized with 0.1% Triton X-100/PBS, blocked, and incubated with secondary Ab. Cell-surface values were expressed as a percentage of the total recycling DMT1-HA for each clone.

Immunostaining. Cells were fixed with 4% paraformaldehyde diluted in PBS for 15−20 min at 20 °C and, where indicated, were permeabilized with 0.1% Triton X-100 in PBS for 30 min at room temperature. Cells were blocked for 30 min in 5% nonfat milk in PBS, followed by consecutive incubations with primary antibodies (mouse anti-HA, 1:500; goat anti-EEA1, 1:100; diluted in blocking solution) and secondary antibodies (goat anti-mouse-Cy3, donkey anti-mouse-alexa Fluor488, and donkey anti-goat-alexa Fluor488; all used at 1:2000) each for 1 h at 20 °C. For experiments with live cells, the anti-HA antibody was diluted (1:200) in 2% nonfat milk in RPMI, and (where indicated) cells were chased by washing twice and incubating the cells in growth media for 90 min at 37 °C. For colocalization with GFP-fusion proteins, cells were transfected 24 h prior to fixation using Lipofectamine2000 (Invitrogen) according to the instructions of the manufacturer. Cells were visualized using a Leica IRE DR2 microscope using a 100× oil immersion objective. Digital images were acquired with an Orca II ER camera (Hamamatsu) operated with the Openlab 3 software (Improvision) installed on an Apple G4 computer. Images were cropped, assembled, and labeled using Adobe Photoshop software.

Cell-Surface Biotinylation. Cell-surface biotinylation was performed based on a similar technique used to study the internalization of CFTR (*31*). LLC-PK_1 cells were grown in 100 mm culture dishes for 1 day postconfluency, followed by 2 washes in PBS++ and one with cold borate buffer at pH 9.0 (10 mM boric acid, 154 mM NaCl, 7.2 mM KCl, and 1.8 mM $CaCl_2$). Cells were biotinylated for 1 h at 4 °C in borate buffer containing 0.7−1.0 mg/mL sulfo-NHS-SS-biotin (Pierce). After two 5 min washes with cold RPMI, cells were incubated in prewarmed RPMI for 0, 30, 60, or 90 min at 37 °C in 5% CO_2, at which point endocytosis was halted by three washes with cold PBS++. Cell-surface-associated biotin molecules were removed (3 washes, 30 min each at 4 °C) by treating with the membrane impermeable reducing agent 2-mercaptoethanesulfonic acid (MESNA, 100 mM solution with 50 mM Tris-HCl at pH 8.6, 1 mM $MgCl_2$, and 0.1 mM $CaCl_2$). For quantification of total surface labeling, cells were similarly treated but with final washes in buffer lacking MESNA. Biotinylated cells were collected and solubilized for 30 min on ice in 350 μL of lysis buffer (1% Triton X-100, 0.2% SDS, 50 mM Tris-HCl at pH 7.4, 150 mM NaCl, and 20% glycerol) supplemented with protease inhibitors (1 mM phenylmethylsulfonyl fluoride, 1 μM pepstatin, 0.3 μM aprotinin, and 1 μM leupeptin). Lysates were precleared by centrifugation (10000*g* at 4 °C for 20 min), and proteins in the supernatant were quantified by the Bradford assay (BioRad). Biotinylated proteins (250 μg of total protein lysate) were isolated by overnight incubation at 4 °C of 100 μL of ImmunoPure immobilized strepavidin slurry (Pierce) in a final volume of 1 mL in lysis buffer with protease inhibitors. Strepavidin beads were washed 4 times with cold lysis buffer, and bound proteins were eluted with 2× Laemmli buffer at room temperature for 30 min. Proteins were separated by SDS−PAGE followed by immunoblotting with anti-HA Ab. Intensities of immunoreactive bands were quantified by densitometry analysis of exposed films using a Fuji LAS-1000. Background intensity readings (after 0 min of endocytosis) were subtracted from all readings, and results were expressed as a percentage of the total surface labeling for each clone.

RESULTS

Expression and Functional Characterization of DMT1 Mutants. To identify sequences involved in plasma-membrane internalization via recycling endosomes, DMT1 isoform II (−IRE, 1B) mutants having independent deletions of the amino terminus (ΔNT), the carboxyl terminus (ΔCT), as well as NPAY (ΔNPAY), YSCF (ΔYSCF), and YLLNT (ΔYLLNT) signatures were made (Figure 1B). A mouse *DMT1* (isoform II) cDNA backbone was used for mutagenesis, after modification by insertion of an exofacial hemag-

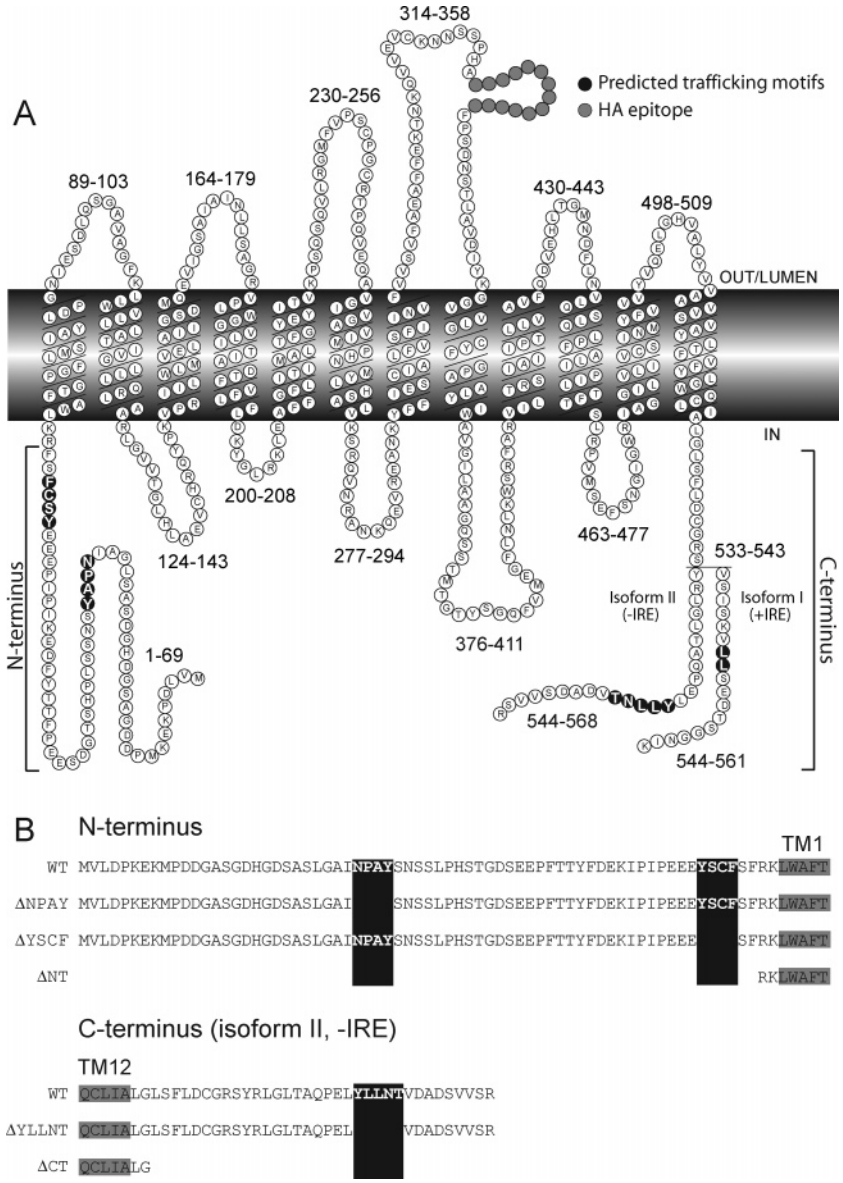

FIGURE 1: Predicted structural features and membrane topology of DMT1. (A) Schematic representation and membrane topology for mouse DMT1 isoforms I (containing an IRE; +IRE; 1A) and II (−IRE; 1B). The amino acid sequence of two isoforms (I and II) is shown. The position and boundaries of the 12 predicted TM domains and corresponding intra- and extracytoplasmic loops are shown. Highlighted are the positions of the antigenic HA epitope tag inserted between TM7 and TM8 (gray) and the predicted targeting/sorting sequence motifs (black). (B) Schematic representation of mutants harboring deletions of predicted targeting/sorting sequence motifs in the amino (N) and carboxyl (C) termini of mouse DMT1 isoform II tested in this study. Predicted targeting motifs (black) and TM domains 1 and 12 (gray) are highlighted.

glutinin (HA) tag into the 4th predicted extracellular loop (delineated by TM7-8; Figure 1A). This enabled recognition of cell-surface-expressed DMT1 molecules in intact cells. Insertion of an HA tag at this position affects neither expression, transport activity, nor subcellular localization of DMT1 (*7*). All *DMT1* mutants were stably transfected in the porcine kidney proximal tubule cell line LLC-PK_1, and clones stably expressing individual mutants were isolated. LLC-PK_1 cells were chosen because they are derived from the proximal tubule, an abundant site of DMT1 protein expression (*15*). These cells are expected to express the necessary machinery and proteins for DMT1 sorting, including recognition of DMT1 targeting and sorting signals. Immunoblot analysis of whole cell extracts (Figure 2A) prepared from the wild type (WT) and the DMT1-HA mutants ΔNPAY, ΔYSCF, and ΔYLLNT displayed two immunoreactive bands of ∼60 and ∼90 kDa, corresponding to the core and complex-glycosylated forms of DMT1, respectively (*7*). The C-terminal deletion (ΔCT) was also expressed as two immunoreactive variants of slightly faster electrophoretic mobility, consistent with the deletion of the 34 C-terminal residues. Thus, ΔCT, ΔNPAY, ΔYSCF, and ΔYLLNT can be expressed and glycosylated in LLC-PK_1 cells. The ΔNT construct was expressed as a ∼55-kDa variant (Figure 2A), the predicted size of the unglycosylated truncated species (*5*, *7*), suggesting that the N-terminal cytoplasmic domain of DMT1 is essential for proper processing and post-translational modification of the protein.

The ability of the DMT1 variants to transport Fe^{2+} and Co^{2+} at acidic pH (pH 6.0) was tested using a fluorescence-quenching assay (*2*, *30*). LLC-PK_1 transfectants were loaded with the metal-sensitive fluorescent dye calcein, and the

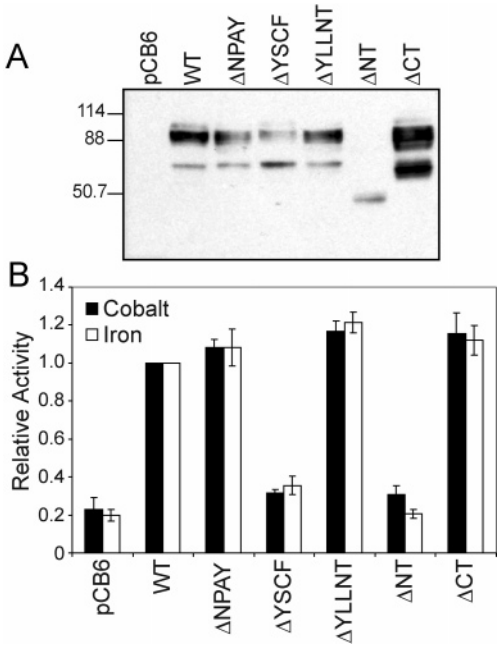

FIGURE 2: Expression and metal transport activity of DMT1-HA mutants in transfected LLC-PK$_1$ cells. (A) Total cell extracts from LLC-PK$_1$ cells stably transfected with either vector alone (pCB6), wild-type DMT1-HA (WT), or various DMT1-HA deletion mutants (identified) were quantified by the Bradford protein assay, and 25 μg of each lysate was separated by SDS−PAGE, followed by immunoblotting with an anti-HA monoclonal antibody. The sizes of the molecular-mass markers are indicated. (B) Metal-transport activity by WT and mutant DMT1 variants was tested using a fluorescence quenching assay. Cells loaded with the metal-sensitive fluorescent dye calcein were incubated with Fe^{2+} or Co^{2+} in acidic buffer (pH 6.0), and the rate of fluorescence quenching was measured over time. The slopes from initial quenching curves were calculated, and transport activity of the mutants was expressed as a percentage of WT activity (relative activity). Error bars = standard error of the means of three or more independent experiments.

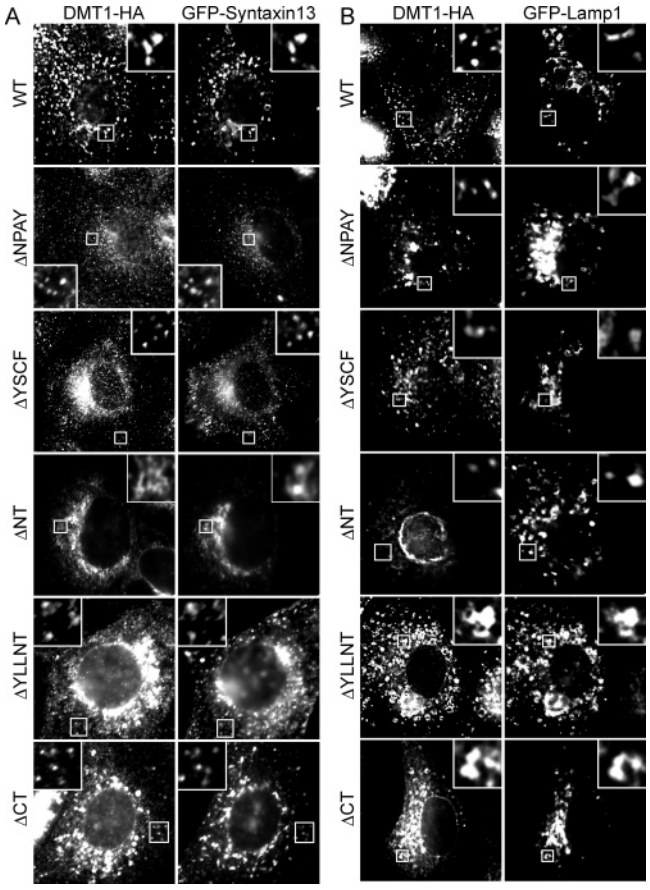

FIGURE 3: Subcellular distribution of WT and mutant DMT1-HA in endomembrane compartments. LLC-PK$_1$ cells stably expressing WT or mutant DMT1-HA variants (identified) were transiently transfected with either GFP-syntaxin 13 (A) to label recycling endosomes or GFP-Lamp1 (B) to label lysosomes. After 24 h, cells were fixed, permeabilized, and stained with a monoclonal anti-HA antibody. DMT1-HA molecules were visualized using a secondary anti-mouse Ab coupled to fluorescent Cy3. Images were acquired by epifluorescence microscopy. Insets show magnifications of the area boxed in the figure.

effect of externally added metal on the rate of fluorescence quenching was measured and compared to that of WT DMT1 (Figure 2B). DMT1 variants ΔNPAY, ΔYLLNT, and ΔCT were fully active for Fe^{2+} and Co^{2+} transport, suggesting that they are expressed at the cell surface and are properly folded in a transport-competent conformation. Cells expressing variants ΔYSCF and ΔNT showed no activity, displaying transport rates similar to cells transfected only with the empty vector (Figure 2B). These results suggest that ΔYSCF and ΔNT are either transport inactive and/or are not efficiently targeted to the proper transport site (plasma membrane and/or recycling endosomes).

Subcellular Localization. To determine whether the mutations that we introduced affected DMT1 targeting, the subcellular localization of the different variants was determined by immunoflurescence using an anti-HA monoclonal antibody. In fixed and permeabilized cells, wild-type DMT1-HA fluorescence was detected as a punctate and juxtanuclear pattern (Figure 3A) (*5*, *7*). Having previously shown that DMT1-HA isoform II is present and active in syntaxin 13-positive recycling endosomes (*7*), we examined the effect of the different mutations on targeting to this compartment. Recycling endosomes were labeled by transient transfection of a GFP-syntaxin 13 construct, and DMT1-HA variants were visualized using a secondary antibody coupled to Cy3 (Figure 3A). The ΔNPAY and ΔYSCF variants showed extensive colocalization with syntaxin 13 and shared a pattern similar to that seen for WT DMT1-HA. ΔNPAY and ΔYSCF also showed extensive costaining with a GFP-transferrin receptor construct (data not shown), confirming that these variants are present in recycling endosomes. These results indicate that the cytoplasmic motifs NPAY and YSCF do not play a major role in targeting DMT1 to early and recycling endosomes. In contrast, the ΔNT variant showed no significant colocalization with GFP-syntaxin 13 and distributed in a more perinuclear pattern possibly corresponding to the endoplasmic reticulum (Figure 3A). The ΔYLLNT and ΔCT variants showed some overlap with GFP-syntaxin 13 (Figure 3A) and with GFP-transferrin receptor (data not shown). However, there was a significant fraction of ΔYLLNT and ΔCT that did not colocalize with the recycling endosome markers.

To determine if any of the mutants were mistargeted to late endosomes and/or lysosomes, we labeled these organelles by transient transfection with a GFP-Lamp1 construct. WT DMT1-HA, as well as the ΔNPAY and ΔYSCF variants showed no significant costaining with GFP-Lamp1. These results are consistent with the extensive colocalization of WT, ΔNPAY, and ΔYSCF with recycling endosomes (Figure 3A). The ΔNT variant similarly did not colocalize with GFP-

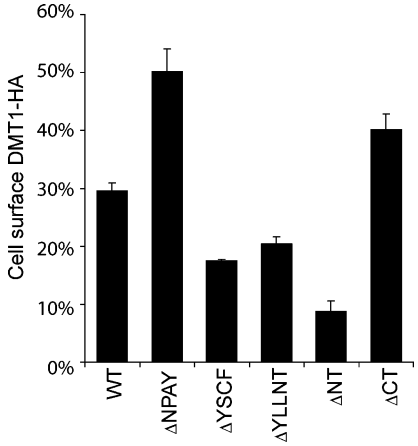

FIGURE 4: Quantification cell-surface DMT1-HA expression at steady state. LLC-PK_1 cells stably expressing individual DMT1-HA variants were fixed and incubated with anti-HA primary antibody with or without prior detergent permeabilization (see the Materials and Methods). Cells were then incubated with an HRP-coupled secondary anti-mouse antibody, and the amount of bound primary antibody present was determined for both conditions by a colorimetric reaction using OPD followed by spectrometry. The amount of DMT1-HA expressed at the cell surface (in nonpermeabilized cells) is shown as a fraction (%) of total protein expression (in permeabilized cells).

Lamp1 positive lysosomes (Figure 3B). These results suggest that the N terminus of DMT1 is essential for proper targeting, and its deletion results in a protein that is not properly glycosylated (Figure 2A), nonfunctional (Figure 2B), and mistargeted to a perinuclear compartment (parts A and B of Figure 3). In contrast to the WT and other DMT1-HA variants, ΔYLLNT and ΔCT both displayed significant costaining with GFP-Lamp1 lysosomes (Figure 3B). These results suggest that the C terminus of DMT1-HA contains information that is critical for optimal targeting of the transporter to recycling endosomes and that deletion of this information results in mistargeting of the protein to late endosomes/lysosomes.

Determinants of Expression at the Cell Surface and in the Recycling Compartment. We next examined the effect of the mutations on the (a) targeting of DMT1 to the cell surface and (b) dynamic trafficking through the recycling endosome compartment. The fraction of each DMT1-HA variant present at the cell surface at steady state was determined by exposing fixed LLC-PK_1 transfectants to anti-HA antibody, with or without prior permeabilization with mild detergent. The amount of bound anti-HA antibody was quantified using a secondary antibody coupled to horseradish peroxidase. WT DMT1-HA transfectants expressed 29.5 ± 1.4% (mean ± SE) of the total DMT1-HA at their cell surface (Figure 4), which is comparable to the fraction that we previously determined using radiolabeled antibodies (*7*). A significantly higher proportion of variants ΔNPAY and ΔCT was detected at the cell surface (50.1 ± 3.9 and 40.2 ± 2.7%, respectively), while the ΔYSCF and ΔYLLNT variants showed a lower fraction of cell-surface expression (17.5 ± 0.2 and 20.5 ± 1.2%, respectively). Finally, only a small fraction of the ΔNT variant was expressed at the cell surface (8.8 ± 1.8%). These results suggest that defined sequences in the amino- and carboxyl-terminal domains of DMT1 play a role in determining the level of DMT1 protein expression at the plasma membrane at steady state.

Because immunofluorescence studies (Figure 3) indicated that certain variants had a larger fraction of protein associated with either a perinuclear compartment (ΔNT) or with lysosomes (ΔYLLNT and ΔCT), we attempted to visualize the proportion of the recycling pool of WT and variant DMT1-HA that is expressed at the cell surface. For this, live LLC-PK_1 transfectants were incubated with anti-HA antibody (2 h, 37 °C), followed by fixation and incubation with a secondary anti-mouse antibody coupled to a red fluorophore to label DMT1-HA proteins at the cell surface. The same cells were then permeabilized under mild detergent conditions, and total DMT1-HA molecules were labeled with a secondary anti-mouse antibody coupled to a green fluorophore. In these experiments, DMT1-HA molecules at the cell surface are labeled in red, while total molecules were labeled in green, with the yellow color in merged images corresponding to the fraction of total labeled DMT1-HA molecules expressed at the cell surface (Figure 5A). This protocol selectively labels only those DMT1-HA molecules that were internalized from the plasma membrane within 2 h, allowing a better determination of the proportion of DMT1-HA at the cell surface versus the intracellular recycling pool. These studies showed that only a small proportion of labeled DMT1-HA is expressed at the cell surface for WT and ΔYSCF, with the majority of protein appearing to be intracellular (Figure 5A). On the contrary, in cells expressing variants ΔNPAY, ΔYLLNT, and ΔCT, a significantly larger proportion of the protein appears to be at the cell surface (yellow staining in Figure 5A). Results for variants ΔNPAY and ΔCT are consistent with the higher expression at the surface detected for these mutants in Figure 4. On the other hand, the high association of ΔYLLNT with the lysosomes noted in Figure 3B may be responsible for the apparent lower surface expression noted in Figure 4. Cells expressing the ΔNT variant showed little if any surface labeling by this method, in agreement with the almost complete association of this mutant with the a perinuclear compartment noted in Figure 3.

The higher proportion of cell-surface expression from the total recycling pool detected for variants ΔNPAY, ΔYLLNT, and ΔCT by immunofluorescence (Figure 5B) was further quantified by an ELISA-based assay as described in the Materials and Methods. In the case of WT DMT1-HA, 19.3 ± 4.8% of the labeled recycling compartment was expressed at the cell surface, and similar results were obtained for the ΔYSCF variant (21.7 ± 5.1%). On the other hand and in agreement with results in Figure 5A, the ΔNPAY, ΔYLLNT, and ΔCT constructs showed a significantly higher distribution of this recycling pool to the cell surface (38.8 ± 2.4, 49.0 ± 2.0, and 60.0 ± 1.6%, respectively). The low level of expression of the ΔNT variant in the recycling pool precluded a similar analysis of this mutant. It is important to note that the extent of surface expression determined for DMT1-HA in intact cells (Figure 5) was somewhat lower than that determined in fixed cells (Figure 4). Therefore, results in Figure 5 may be an underestimate of the actual surface expression of DMT1-HA because of incomplete inaccessibility of the HA epitope in native, unfixed cells. However, this does not affect direct comparisons between WT and mutant DMT1-HA expressing cells by either method.

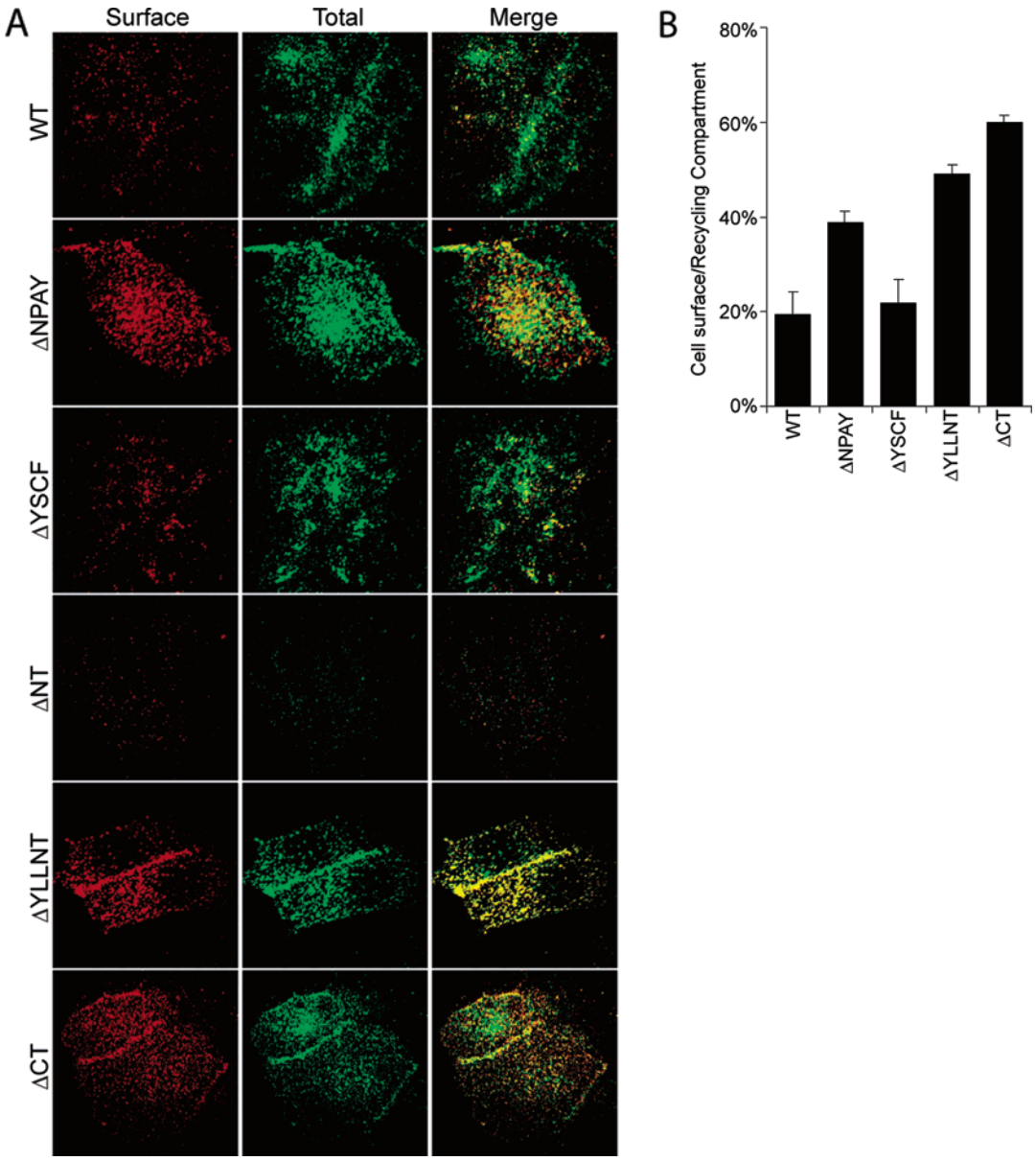

FIGURE 5: Determination of the fraction of the recycling pool expressed at the cell surface for each DMT1-HA variant. (A) Dual labeling of cell surface expressed (surface; red) and total recycling pool (total; green) of DMT1-HA variants, with the overlap (merge; yellow) identifying the fraction of the recycling pool expressed at the cell surface. LLC-PK_1 cells stably expressing WT or mutant DMT1-HA were incubated with anti-HA Ab for 2 h at 37 °C to label recycling DMT1-HA molecules. After incubation, cells were fixed and incubated with a secondary anti-mouse antibody coupled to Cy3 (red) to label cell-surface DMT1-HA molecules. After washing, cells were permeabilized with detergent and incubated with a secondary anti-mouse antibody coupled to Alexa488 (green) to label total recycling DMT1-HA molecules (plasma membrane plus endosomes). Images were compiled from 0.5 μm confocal microscopy *z*-plane sections. (B) Quantification of the fraction of the recycling pool of the DMT1-HA variants expressed at the cell surface. The recycling pool and fraction of the recycling pool expressed at the cell surface for each DMT1-HA variant was labeled as described in A, except that an HRP conjugate was used as a secondary antibody for quantification. Results are expressed as the fraction (%) of the total recycling pool of each mutant expressed at the cell surface. Error bars correspond to standard errors on the means from three or more independent experiments.

Together, the results in Figures 4 and 5 indicate that the NPAY motif in the amino-terminal domain and sequences in the C-terminal domain of DMT1 (including YLLNT) play an important role in directing the traffic of the transporter to and/or from the plasma membrane.

Endocytosis. The noted cell-surface accumulation of variants ΔNPAY, ΔYLLNT, and ΔCT suggested a potential defect in internalization of these mutants from the plasma membrane. To test this possibility, we used a cell-surface biotinylation assay to compare the rates of endocytosis of WT and mutant DMT1 variants ΔYLLNT, ΔNPAY, and ΔCT. A similar approach has been previously used to study internalization kinetics of other membrane proteins such as CFTR (*31*) and the H,K-ATPase (*32*). We used a cleavable form of biotin (NHS-SS-biotin) to covalently label lysine residues in proteins exposed at the extracellular surface. LLC-PK_1 cell monolayers were biotinylated at 4 °C to arrest membrane endocytosis. After cell-surface biotinylation, we raised the temperature of the medium to 37 °C for 0−90 min to allow internalization of plasma-membrane constituents. Biotin molecules remaining at the cell surface were cleaved by washing the cells with the membrane-impermeant reducing agent MESNA. After cell lysis, biotinylated DMT1-HA molecules were isolated using immobilized streptavidin, followed by SDS−PAGE and immunoblotting with anti-HA antibody. A typical immunoblot is shown in Figure 6A, while

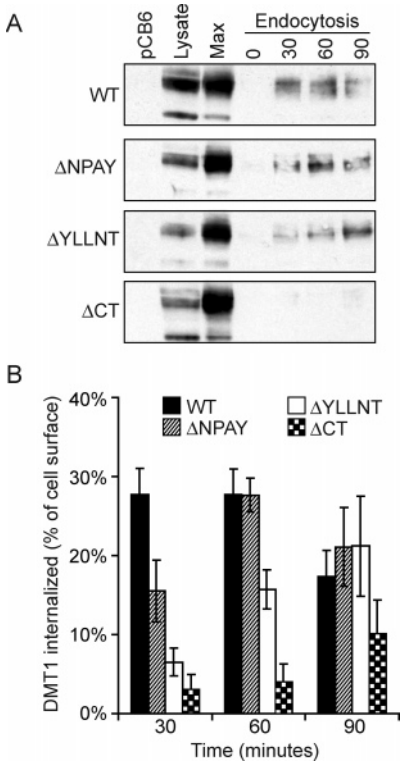

FIGURE 6: Internalization of DMT1-HA variants from the cell surface. A cell-surface biotinylation assay was used to determine the rate of endocytosis of WT and variant DMT1-HA molecules from the plasma membrane. We used a cleavable form of biotin to covalently label the ϵ-amino groups of lysine residues of all cell-surface proteins (see the Materials and Methods). LLC-PK_1 transfectants expressing either WT or ΔNPAY, ΔYLLNT, and ΔCT mutant DMT1-HA were labeled with biotin at 4 °C to halt endocytosis. After washes, the temperature of the medium was raised to 37 °C followed by incubation for 0−90 min to allow the internalization of plasma-membrane constituents. Biotin molecules remaining at the cell surface were cleaved with a membrane-impermeant reducing agent. Biotinylated DMT1-HA molecules were isolated from cell lysates with immobilized strepavidin, followed by elution with sample buffer and analysis by SDS−PAGE and immunoblotting with anti-HA Ab. Typical immunoblots from individual experiments are shown in A. Lysate = 20 μg of unbiotinylated crude cell lysate for each mutant. Max = total surface DMT1-HA expression for each mutant (biotinylated DMT1-HA molecules isolated without prior stripping). (B) Quantification of rates of internalization of DMT1-HA variants from the plasma membrane. Immunoblots were scanned by densitometry, and the amount of DMT1 internalized over time is expressed as a fraction (%) of the total cell-surface expression (max). Error bars correspond to standard errors on the means from three or more independent experiments.

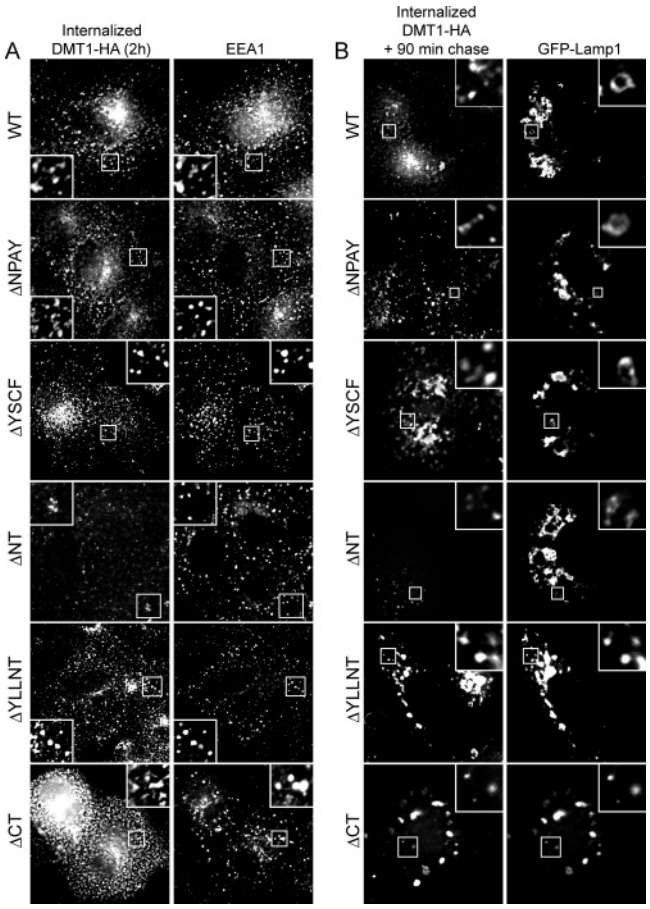

FIGURE 7: Subcellular localization of internalized DMT1-HA molecules. (A) LLC-PK_1 transfectants expressing either WT or mutant DMT1-HA (identified) were incubated with anti-HA Ab for 2 h to label cell-surface and recycling DMT1-HA molecules. Cells were fixed, permeabilized, and incubated with an antibody against the early endosomal marker EEA1. (B) LLC-PK_1 cells were transiently transfected with the lysosomal marker GFP-Lamp1. After 24 h, surface and recycling DMT1-HA molecules were labeled with anti-HA Ab for 3 h, washed, and chased by incubation in growth media for 90 min at 37 °C. Cells were fixed, permeabilized, and stained with an anti-mouse secondary Ab to visualize DMT1-HA molecules. Images were acquired by epifluorescence microscopy. Insets show magnifications of the area boxed in the figure.

quantification from different immunoblots ($n \geq 3$) by densitometry scanning is shown in Figure 6B. In these experiments, controls for equal amounts of labeled lysates introduced in the capture assay (lysate from cells untreated with MESNA) and transferred to membrane (max) were included for normalization purposes. Using this method, 27.7 ± 3.3% (mean ± SE) of surface-labeled DMT1-HA was internalized after 30 min (Figure 6B). Mutant ΔNPAY showed reduced internalization, with 15.7 ± 3.9% after 30 min, but the difference from the WT became insignificant after 60 min. On the other hand, mutant ΔYLLNT displayed a more severe deficiency in DMT1-HA internalization (6.5 ± 1.8% internalization after 30 min and 15.7 ± 2.5% after 60 min), while the ΔCT appeared to be completely impaired in this process, with little if any internalization detected (3.0 ± 1.9% after 30 min and 4.0 ± 2.3% after 60 min) (Figure 6B). These results indicate that the C terminus of DMT1 contains information (including the YLLNT motif) that is essential for rapid endocytosis from the plasma membrane, and consequently, mutations in this region lead to accumulation of DMT1 at the cell surface.

The Fate of Internalized DMT1 Molecules. We next investigated whether, once internalized, WT and variant DMT1-HA were targeted to the same endomembrane compartments. To test this, we incubated live LLC-PK_1 cells with anti-HA Ab for 2 h at 37 °C to label surface and recently internalized DMT1-HA molecules. After fixation and permeabiliztion, we labeled early endosomes with an antibody against the early endosome marker EEA1. WT DMT1-HA showed significant costaining with EEA1 (Figure 7A), consistent with previous studies with DMT1 isoform II (−IRE, 1B) (*7*, *14*). Interestingly, all variants tested also displayed significant costaining with EEA1 after 2 h (Figure 7A), with the exception of ΔNT, which showed no costaining

with EEA1 and little anti-HA antibody incorporation. To determine the fate of internalized WT and variant DMT1-HA molecules after a longer incubation period, live LLC-PK_1 cells were labeled with anti-HA Ab for 3 h at 37 °C. The cells were then washed and chased for an additional 90 min in culture media at 37 °C. Lysosomes were labeled by transient transfection with GFP-Lamp1 at 24 h prior to labeling. WT DMT1-HA as well as variants ΔNPAY and ΔYSCF showed no significant costaining with GFP-Lamp1 lysosomes and retained a similar juxtanuclear staining pattern (Figure 7B). These results suggest that WT, ΔNPAY, and ΔYSCF proteins are stably recycling from the cell surface and are not targeted to the lysosomes within 90 min of internalization. As expected, ΔNT showed little uptake of anti-HA antibody and no costaining with GFP-Lamp1 (Figure 7B). Strikingly, however, the ΔYLLNT and ΔCT variants displayed significant costaining with GFP-Lamp1 lysosomes >90 min after internalization (Figure 7B). These results suggest that the YLLNT motif and possibly other residues in the C terminus of DMT1 isoform II are critical for the recycling of the transporter to the cell surface. Furthermore, this study shows that critical mutations in the C terminus of DMT1 isoform II result in a transporter that is (a) internalized with slower kinetics from the cell surface, (b) not efficiently recycled back to the cell surface, and (c) eventually targeted to the lysosomal compartment.

DISCUSSION

In this study, we sought to identify specific signal(s) in cytoplasmic domains of DMT1 responsible for internalization of the transporter from the plasma membrane into recycling endosomes. Truncation of the amino-terminal domain of DMT1 (ΔNT) had drastic effects on protein expression and targeting. ΔNT was not properly glycosylated, was transport-inactive, and was expressed neither at the plasma membrane nor in syntaxin 13-positive recycling endosomes or Lamp1-positive lysosomes. ΔNT was found almost exclusively in a perinuclear compartment, which was positive for the endoplasmic reticulum marker calnexin (data not shown). These results suggest that an intact amino terminus of DMT1 is essential for processing and stability of the protein.

Deletion of the $NPAY^{28-31}$ motif in the amino terminus of the protein did not have a major effect on either protein function or subcellular targeting. The ΔNPAY variant was transport-competent (Figure 2B) and showed a subcellular distribution indistinguishable from that of WT DMT1 (Figure 3). On the other hand, the ΔNPAY mutant showed increased surface expression (Figure 4), and an increased proportion of the recycling pool was present at the cell surface (Figures 4 and 5) compared to WT. ΔNPAY showed a somewhat slower rate of internalization (Figure 6B). These results raise the possibility that the NPAY motif may further contribute to internalization of DMT1 in LLC-PK_1 cells. However, this motif appears to be of limited importance when compared to signals in the carboxyl terminus of DMT1 (see below). Finally, we cannot exclude the possibility that the NPAY motif may play additional cell-specific roles in targeting and trafficking of DMT1, which may have gone undetected in LLC-PK_1 kidney cells.

Deletion of the other tyrosine-based motif, $YSCF^{62-65}$, did not have a major effect on the subcellular localization of the protein in LLC-PK_1 cells. Similar to WT DMT1, this mutant was limited to plasma-membrane and recycling endosomes (Figure 3). Distribution of the ΔYCSF mutant between the cell surface and endomembranes of the recycling pool was also similar to the WT protein. Thus, the YSCF motif appears to be neither critical for DMT1 targeting nor recycling in LLC-PK_1 cells. However, ΔYSCF was clearly transport-incompetent (Figure 2B), suggesting that some or all of the residues in $YSCF^{62-65}$ are required for transport. This requirement may involve a direct role for these residues in the transport process. However, the lower level of expression of this mutant (Figure 2A) may also contribute to the inactivity of the mutant.

On the other hand, alterations in the predicted carboxyl-terminal intracellular domain of DMT1 had the most dramatic effects on DMT1 targeting and recycling. Truncation of the entire carboxyl-terminal domain (ΔCT) or deletion of the YLLNT (ΔYLLNT) motif did not significantly affect either the level of protein expression in LLC-PK_1 transfectants or their transport properties (Figure 2), suggesting that these regions are not critical for activity or stability. A small fraction of ΔCT and ΔYLLNT was detected in the syntaxin 13-positive recycling endosomes (Figure 3A), suggesting that a part of these variants was properly targeted. However, the C-terminal domain variants showed robust colocalization with Lamp1-positive lysosomes, both at steady state (Figure 3B) and after a transient labeling of internalized DMT1-HA molecules, 90 min after endocytosis (Figure 7B). Interestingly, both ΔCT and ΔYLLNT variants displayed an increased fraction of the "recycling pool" expressed at the cell surface when compared to the WT (Figure 5). This increased accumulation at the plasma membrane may be explained by a defect in internalization of these variants that we measured by surface biotinylation (Figure 6). These results implicate the YLLNT sequence of DMT1 as a critical motif for internalization from the plasma membrane. Other carboxyl-terminal residues of DMT1 may additionally contribute to internalization because truncation of the entire carboxyl terminus causes a more severe defect than that seen in the YLLNT mutant.

Previous studies have shown that WT DMT1 isoform II is rapidly internalized via a clathrin- and dynamin-dependent mechanism and is efficiently targeted back to the cell surface by means of recycling endosomes (*7*). The impaired internalization and accumulation in the lysosomes of the C-terminal domain mutants suggests a model whereby, in the absence of the YLLNT motif, DMT1 is subject to a default lysosomal targeting. In this model (Figure 8), DMT1 recruits specific adaptor proteins required for rapid clathrin-mediated endocytosis through binding to its YLLNT motif. DMT1 is internalized into early endosomes, and the recruited adaptor complexes are involved in signaling the recycling of the transporters back to the cell surface via recycling endosomes (Figure 8). Indeed, proper interaction with clathrin has been previously shown to be critical for internalization and trafficking of certain membrane proteins through recycling endosomes, most notably the transferrin receptor (*33*, *34*). The recruitment of adaptor complexes (Ap1/μ1B) has been shown to be critical for efficient recycling of both the transferrin and LDL receptors to the basolateral membrane in epithelial cells (*35*). In contrast, the C-terminal domain mutants, which lack the YLLNT motif, are unable to recruit

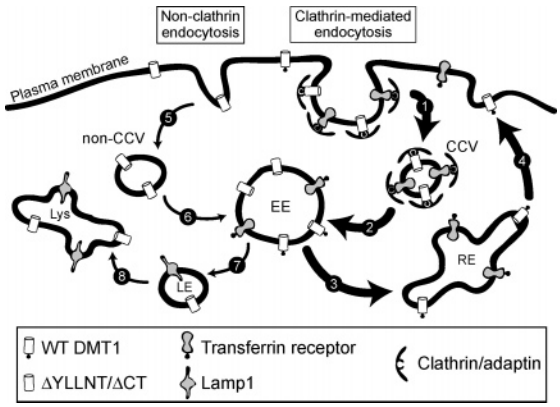

FIGURE 8: Schematic model for endocytosis of cell-surface-expressed WT and C-terminus mutant DMT1 molecules. Clathrin molecules interact with cell-surface DMT1 molecules via adaptins (AP-1 and AP-2) that specifically recognize the tyrosine-based motif YLLNT. This causes formation of DMT1-enriched clathrin-coated pits on the cell surface, which are rapidly internalized (step 1) by a dynamin-dependent process into clathrin-coated vesicles (CCV). DMT1-containing CCVs are then sorted to the early endosome compartment (EE, step 2) and eventually recycled back to the cell surface via sorting to the recycling endosome compartment (RE, steps 3 and 4) along with the transferrin receptor. In contrast, DMT1 C-terminus mutants, which lack the tyrosine-based sorting motif (ΔYLLNT and ΔCT), are internalized less rapidly by a clathrin-independent mechanism (such as bulk pinocytosis) into non-CCVs (step 5) and are sorted to EE (step 6). The mutant DMT1 proteins are recycled much less efficiently compared to the WT and are eventually sorted to the Lamp1-positive late endosome and lysosome compartments (steps 7 and 8).

clathrin/adaptor complexes and are internalized into early endosomes by a kinetically slower mechanism such as bulk pinocytosis (Figure 8). However, the failure of the C-terminus mutants to recruit specific adaptors disrupts their proper sorting to recycling endosomes and leads to an accumulation in lysosomes. Ultimately, our data does not favor the existence of a true lysosomal targeting motif in DMT1 isoform II but rather that the lysosome may be the default pathway for the transporter.

Recently, Tabouchi and colleagues observed that, in transfected HEp-2 larynx carcinoma cells, the DMT1 isoform I is targeted to the late endosome/lysosome compartment, while isoform II is targeted to the early endosomes of these cells (*14*). They demonstrated that the 36 carboxyl-terminal residues of DMT1 isoform II are important for targeting to early endosomes and that alterations in the YXLXX motif (YLLNT) in isoform II impair targeting to early endosomes and cause accumulation of the mutants in Lamp2-positive late endosomes/lysosomes. The authors concluded that the targeting signal for early endosomes dominates over signals for late endosomes/lysosomes in DMT1 isoform II. Our results agree that critical C-terminus mutations in DMT1 isoform II (ΔYLLNT and ΔCT) cause significant colocalization of the transporter with Lamp1/2-positive lysosomes. However, our data suggests that the YLLNT motif is more critical for transporter recycling because, upon internalization of ΔYLLNT/ΔCT from the plasma membrane, there was partial colocalization with EEA1-positive early endosomes but not syntaxin 13-positive recycling endosomes (Figure 7A). Tabuchi and colleagues also showed that the C terminus of DMT1 isoform II, when fused to a plasma-membrane marker (TAC antigen), results in early/recycling endosome targeting. This result is consistent our cell-surface biotinylation data (Figure 6) that shows that the YLLNT motif is also critical for endocytosis from the plasma membrane.

Cytoplasmic dileucine-based (LL) motifs of membrane proteins have been shown to act as signals leading to clathrin-mediated endocytosis in other transporters such as the glucose transporter GLUT4 (*36*) and the copper transporter Menkes (MNK) (*37*−*39*). In most proteins, residues preceding the LL signals appear to dictate the method of clathrin recruitment. Dileucine-based signals usually fit the [DE]XXXL-[LI] or DXXLL consensus motifs. [DE]XXXL[LI] signals are specifically recognized by AP complexes. Conversely, DXXLL signals are recognized by another family of adaptors known as GGAs, a recently described family of ARF-dependent clathrin adaptors (*20*). The residues preceding the dileucine motif in DMT1 isoform II ($ELYLL^{553-557}$) do not correspond to the traditional [DE]XXXL[LI] motif but resemble the DXXLL consensus signature. It has been demonstrated that mutations at either the D or LL residues of the DXXLL cause retention of the mannose-6-phosphate receptor at the cell surface (*40*), a behavior resembling that of DMT1 mutants ΔCT and ΔYLLNT studied here in LLC-PK_1 cells. This suggests that the $ELYLL^{553-557}$ sequence of DMT1 may function as a DXXLL signal. Although the dileucine motif in DMT1 resembles the DXXLL consensus with a glutamate (E) substituting for aspartate (D), it remains to be determined whether they act the same way and whether DMT1 recruits GGAs via this motif. Indeed, previous studies of M6PR mutants have shown that the isoelectric substitution of aspartate in the DXXLL consensus sequence for glutamate is not well-tolerated (*41*). Furthermore, the aspartate in classical DXXLL motifs is generally found in the context of a cluster of acidic residues, which is not the case for the DMT1 dileucine signal. Thus, the DMT1 dileucine motif $ELYLL^{553-557}$ may be a novel functional variant of DXXLL or may represent a novel signal for endocytosis of membrane proteins from the cell surface.

When our results are taken together, they indicate that determinants of the carboxyl-terminus cytoplasmic domain of DMT1 play a critical role in internalization of the protein from the plasma membrane and for recirculation in recycling endosomes. Elimination of these signals impairs internalization and redirects the internalized DMT1 proteins to the lysosomal compartment, which appears to act as a default pathway for such DMT1 variants.

ACKNOWLEDGMENT

This work was supported by a research grant to P. G. from the National Institute of Allergy and Infectious Diseases (RO1 AI35237-10). S. L. is supported by a studentship from the Canadian Institutes of Health Research, and P. G. is a supported by a Distinguished Scientist salary award from the Canadian Institutes of Health Research and is a James McGill Professor of Biochemistry.

REFERENCES

1. Gunshin, H., Mackenzie, B., Berger, U. V., Gunshin, Y., Romero, M. F., Boron, W. F., Nussberger, S., Gollan, J. L., and Hediger, M. A. (1997) Cloning and characterization of a mammalian proton-coupled metal-ion transporter, *Nature 388*, 482−488.
2. Picard, V., Govoni, G., Jabado, N., and Gros, P. (2000) Nramp 2 (DCT1/DMT1) expressed at the plasma membrane transports iron and other divalent cations into a calcein-accessible cytoplasmic pool, *J. Biol. Chem. 275*, 35738−35745.

3. Forbes, J. R., and Gros, P. (2003) Iron, manganese, and cobalt transport by Nramp1 (Slc11a1) and Nramp2 (Slc11a2) expressed at the plasma membrane, *Blood 102*, 1884−1892.
4. Canonne-Hergaux, F., Gruenheid, S., Ponka, P., and Gros, P. (1999) Cellular and subcellular localization of the Nramp2 iron transporter in the intestinal brush border and regulation by dietary iron, *Blood 93*, 4406−4417.
5. Gruenheid, S., Canonne-Hergaux, F., Gauthier, S., Hackam, D. J., Grinstein, S., and Gros, P. (1999) The iron transport protein NRAMP2 is an integral membrane glycoprotein that colocalizes with transferrin in recycling endosomes, *J. Exp. Med. 189*, 831−841.
6. Ponka, P., Beaumont, C., and Richardson, D. R. (1998) Function and regulation of transferrin and ferritin, *Semin. Hematol. 35*, 35−54.
7. Touret, N., Furuya, W., Forbes, J., Gros, P., and Grinstein, S. (2003) Dynamic traffic through the recycling compartment couples the metal transporter Nramp2 (DMT1) with the transferrin receptor, *J. Biol. Chem. 278*, 25548−25557.
8. Fleming, M. D., Trenor, C. C., III, Su, M. A., Foernzler, D., Beier, D. R., Dietrich, W. F., and Andrews, N. C. (1997) Microcytic anaemia mice have a mutation in Nramp2, a candidate iron transporter gene, *Nat. Genet. 16*, 383−386.
9. Fleming, M. D., Romano, M. A., Su, M. A., Garrick, L. M., Garrick, M. D., and Andrews, N. C. (1998) Nramp2 is mutated in the anemic Belgrade (b) rat: Evidence of a role for Nramp2 in endosomal iron transport, *Proc. Natl. Acad. Sci. U.S.A. 95*, 1148−1153.
10. Russell, E. S., Nash, D. J., Bernstein, S. E., Kent, E. L., McFarland, E. C., Matthews, S. M., and Norwood, M. S. (1970) Characterization and genetic studies of microcytic anemia in house mouse, *Blood 35*, 838−850.
11. Edwards, J. A., and Hoke, J. E. (1972) Defect of intestinal mucosal iron uptake in mice with hereditary microcytic anemia, *Proc. Soc. Exp. Biol. Med. 141*, 81−84.
12. Su, M. A., Trenor, C. C., Fleming, J. C., Fleming, M. D., and Andrews, N. C. (1998) The G185R mutation disrupts function of the iron transporter Nramp2, *Blood 92*, 2157−2163.
13. Touret, N., Martin-Orozco, N., Paroutis, P., Furuya, W., Tseung, S. L., Forbes, J., Gros, P., and Grinstein, S. (2004) Molecular and cellular mechanisms underlying iron transport deficiency in microcytic anemia, *Blood 104*, *1526*−*1533*.
14. Tabuchi, M., Tanaka, N., Nishida-Kitayama, J., Ohno, H., and Kishi, F. (2002) Alternative splicing regulates the subcellular localization of divalent metal transporter 1 isoforms, *Mol. Biol. Cell 13*, 4371−4387.
15. Canonne-Hergaux, F., and Gros, P. (2002) Expression of the iron transporter DMT1 in kidney from normal and anemic mk mice, *Kidney Int. 62*, 147−156.
16. Lee, P. L., Gelbart, T., West, C., Halloran, C., and Beutler, E. (1998) The human Nramp2 gene: Characterization of the gene structure, alternative splicing, promoter region, and polymorphisms, *Blood Cells Mol. Dis. 24*, 199−215.
17. Hubert, N., and Hentze, M. W. (2002) Previously uncharacterized isoforms of divalent metal transporter (DMT)-1: Implications for regulation and cellular function, *Proc. Natl. Acad. Sci. U.S.A. 99*, 12345−12350.
18. Frazer, D. M., Wilkins, S. J., Becker, E. M., Vulpe, C. D., McKie, A. T., Trinder, D., and Anderson, G. J. (2002) Hepcidin expression inversely correlates with the expression of duodenal iron transporters and iron absorption in rats, *Gastroenterology 123*, 835−844.
19. Canonne-Hergaux, F., Zhang, A. S., Ponka, P., and Gros, P. (2001) Characterization of the iron transporter DMT1 (NRAMP2/DCT1) in red blood cells of normal and anemic mk/mk mice, *Blood 98*, 3823−3830.
20. Bonifacino, J. S., and Traub, L. M. (2003) Signals for sorting of transmembrane proteins to endosomes and lysosomes, *Annu. Rev. Biochem. 72*, 395−447.
21. Goldstein, J. L., Basu, S. K., Brunschede, G. Y., and Brown, M. S. (1976) Release of low-density lipoprotein from its cell surface receptor by sulfated glycosaminoglycans, *Cell 7*, 85−95.
22. Chen, W. J., Goldstein, J. L., and Brown, M. S. (1990) NPXY, a sequence often found in cytoplasmic tails, is required for coated pit-mediated internalization of the low-density lipoprotein receptor, *J. Biol. Chem. 265*, 3116−3123.
23. Pietrzik, C. U., Busse, T., Merriam, D. E., Weggen, S., and Koo, E. H. (2002) The cytoplasmic domain of the LDL receptor-related protein regulates multiple steps in APP processing, *EMBO J. 21*, 5691−5700.
24. Prigent, S. A., and Gullick, W. J. (1994) Identification of c-erbB-3 binding sites for phosphatidylinositol 3′-kinase and SHC using an EGF receptor/c-erbB-3 chimera, *EMBO J. 13*, 2831−2841.
25. Takeda, T., Yamazaki, H., and Farquhar, M. G. (2003) Identification of an apical sorting determinant in the cytoplasmic tail of megalin, *Am. J. Physiol. Cell Physiol. 284*, C1105−C1113.
26. Ohno, H., Stewart, J., Fournier, M. C., Bosshart, H., Rhee, I., Miyatake, S., Saito, T., Gallusser, A., Kirchhausen, T., and Bonifacino, J. S. (1995) Interaction of tyrosine-based sorting signals with clathrin-associated proteins, *Science 269*, 1872−1875.
27. Boll, W., Ohno, H., Songyang, Z., Rapoport, I., Cantley, L. C., Bonifacino, J. S., and Kirchhausen, T. (1996) Sequence requirements for the recognition of tyrosine-based endocytic signals by clathrin AP-2 complexes, *EMBO J. 15*, 5789−5795.
28. Honing, S., Griffith, J., Geuze, H. J., and Hunziker, W. (1996) The tyrosine-based lysosomal targeting signal in lamp-1 mediates sorting into golgi-derived clathrin-coated vesicles, *EMBO J. 15*, 5230−5239.
29. Urbatsch, I. L., Julien, M., Carrier, I., Rousseau, M. E., Cayrol, R., and Gros, P. (2000) Mutational analysis of conserved carboxylate residues in the nucleotide binding sites of P-glycoprotein, *Biochemistry 39*, 14138−14149.
30. Lam-Yuk-Tseung, S., Govoni, G., Forbes, J., and Gros, P. (2003) Iron transport by Nramp2/DMT1: pH regulation of transport by 2 histidines in transmembrane domain 6, *Blood 101*, 3699−3707.
31. Lukacs, G. L., Segal, G., Kartner, N., Grinstein, S., and Zhang, F. (1997) Constitutive internalization of cystic fibrosis transmembrane conductance regulator occurs via clathrin-dependent endocytosis and is regulated by protein phosphorylation, *Biochem. J. 328* (part 2), 353−361.
32. Duffield, A., Kamsteeg, E. J., Brown, A. N., Pagel, P., and Caplan, M. J. (2003) The tetraspanin CD63 enhances the internalization of the H,K-ATPase β-subunit, *Proc. Natl. Acad. Sci. U.S.A. 100*, 15560−15565.
33. Nesterov, A., Carter, R. E., Sorkina, T., Gill, G. N., and Sorkin, A. (1999) Inhibition of the receptor-binding function of clathrin adaptor protein AP-2 by dominant-negative mutant mu2 subunit and its effects on endocytosis, *EMBO J. 18*, 2489−2499.
34. van Dam, E. M., and Stoorvogel, W. (2002) Dynamin-dependent transferrin receptor recycling by endosome-derived clathrin-coated vesicles, *Mol. Biol. Cell 13*, 169−182.
35. Gan, Y., McGraw, T. E., and Rodriguez-Boulan, E. (2002) The epithelial-specific adaptor AP1B mediates post-endocytic recycling to the basolateral membrane, *Nat. Cell Biol. 4*, 605−609.
36. Yeh, J. I., Verhey, K. J., and Birnbaum, M. J. (1995) Kinetic analysis of glucose transporter trafficking in fibroblasts and adipocytes, *Biochemistry 34*, 15523−15531.
37. Petris, M. J., and Mercer, J. F. (1999) The Menkes protein (ATP7A; MNK) cycles via the plasma membrane both in basal and elevated extracellular copper using a C-terminal di-leucine endocytic signal, *Hum. Mol. Genet. 8*, 2107−2115.
38. Petris, M. J., Camakaris, J., Greenough, M., LaFontaine, S., and Mercer, J. F. (1998) A C-terminal di-leucine is required for localization of the Menkes protein in the trans-golgi network, *Hum. Mol. Genet. 7*, 2063−2071.
39. Francis, M. J., Jones, E. E., Levy, E. R., Martin, R. L., Ponnambalam, S., and Monaco, A. P. (1999) Identification of a di-leucine motif within the C terminus domain of the Menkes disease protein that mediates endocytosis from the plasma membrane, *J. Cell Sci. 112* (part 11), 1721−1732.
40. Johnson, K. F., and Kornfeld, S. (1992) The cytoplasmic tail of the mannose 6-phosphate/insulin-like growth factor-II receptor has two signals for lysosomal enzyme sorting in the golgi, *J. Cell Biol. 119*, 249−257.
41. Chen, H. J., Yuan, J., and Lobel, P. (1997) Systematic mutational analysis of the cation-independent mannose 6-phosphate/insulin-like growth factor II receptor cytoplasmic domain. An acidic cluster containing a key aspartate is important for function in lysosomal enzyme sorting, *J. Biol. Chem. 272*, 7003−7012.

BI050911R